REVISION 1

In situ dehydration behavior of veszelyite $(Cu,Zn)_2Zn(PO_4)(OH)_3 \cdot 2H_2O$: A single-crystal X-ray study

ROSA MICAELA DANISI* [a)], THOMAS ARMBRUSTER [a)], BILJANA LAZIC [a)], PREDRAG VULIĆ [b)], REINHARD KAINDL [c), d)], RADOVAN DIMITRIJEVIĆ [b)], VOLKER KAHLENBERG [d)]

[a)] Mineralogical Crystallography, Institute of Geological Sciences, University of Bern, Freiestrasse 3, 3012 Bern, Switzerland

[b)] Laboratory of Crystallography, Faculty of Mining and Geology, University of Belgrade, Djusina 7, 11000 Belgrade, Serbia.

[c)] MATERIALS - Institute for Surface Technologies and Photonics, JOANNEUM RESEARCH, Leobner Strasse 94, 8712 Niklasdorf, Austria

[d)] Institute of Mineralogy and Petrography, University of Innsbruck, Innrain 52f, 6020 Innsbruck, Austria.

*Corresponding author. E-mail address: rosa.danisi@krist.unibe.ch

ABSTRACT

The rare mixed copper-zinc phosphate mineral veszelyite $(Cu,Zn)_2Zn(PO_4)(OH)_3 \cdot 2H_2O$ (space group $P2_1/c$, $a = 7.5096(2)$, $b = 10.2281(2)$, $c = 9.8258(2)$ Å, $\beta = 103.3040(10)°$, $V = 734.45(3)$ Å^3) was investigated by in situ temperature dependent single-crystal X-ray structure refinements. The atomic arrangement of veszelyite consists of an alternation of octahedral and tetrahedral sheets. The Jahn-Teller distorted CuO_6 octahedra form sheets with eight-membered rings. The tetrahedral sheet composed of PO_4 and $ZnO_3(OH)$ tetrahedra shows strong topological similarities to that of cavansite, gismondine and kipushite.

Diffraction data of a sample from Zdravo Vrelo, near Kreševo (Bosnia and Herzegovina) have been measured in steps of 25 up to 225 °C. Hydrogen positions and the hydrogen-bond system were determined experimentally from the structure refinements of data collected up to 125 °C. At 200 °C the hydrogen-bonding scheme was inferred from bond-valence calculations and donor-acceptor distances. The hydrogen-bond system connects the tetrahedral sheet to the octahedral sheet and also braces the Cu sheet.

At 150 °C the H_2O molecule at H_2O2 was released and the Cu coordination (Cu1 and Cu2) declined from originally six- to five-fold. Cu1 has a square planar coordination by four OH groups and an elongate distance to O3 whereas Cu2 has the Jahn-Teller characteristic elongate

bond to H_2O1. The unit-cell volume decreased 7% from originally 734.45(3) $Å^3$ to 686.4(4) $Å^3$ leading to a formula with 1 H_2O pfu. The new phase observed above 150 °C is characterized by increase of the **c** axis and a shortening of the **b** axis. The bending of T-O-T angles causes increasing elliptical shape of the eight-membered rings in the tetrahedral and octahedral sheets. Moreover a rearrangement of the hydrogen-bond system was observed.

At 225 °C the structure degrades to an X-ray amorphous residual due to release of the last H_2O molecule at H_2O1. The stronger Jahn-Teller distortion of Cu1 relative to Cu2 suggests that Cu1 is fully occupied by Cu whereas Cu2 bears significant Zn. H_2O1 is the fifth ligand of Cu2. Zn at Cu2 is not favorable to adopt planar four-fold coordination. Thus, if the last water molecule is expelled the structure is destabilized.

This study contributes to understanding the dehydration mechanism and thermal stability of supergene minerals characterized by Jahn-Teller distorted octahedra with mixed Cu, Zn occupancy.

KEYWORDS: Veszelyite, Jahn-Teller effect, dehydration, crystal structure, hydrogen bonding.

1. INTRODUCTION

Veszelyite, $(Cu,Zn)_2Zn(PO_4)(OH)_3{\cdot}2H_2O$, is a rare mixed copper-zinc phosphate mineral named after A. Veszeli (1820-1888), a Hungarian mining engineer, who discovered the species.

The atomic arrangement of veszelyite consists of an alternation of octahedral and tetrahedral sheets (Ghose et al. 1974). The octahedral sheet is made up of distorted $Cu^{2+}O_6$ octahedra joined to form a network of eight-membered rings parallel to the **b** - **c** plane. The tetrahedral sheet is composed by alternating PO_4 and $ZnO_3(OH)$ tetrahedra forming undulating pyroxenoid-like chains extended parallel to **c**. Adjacent chains have the tetrahedral apices pointing alternatively up and down along the **a** axis. These chains are laterally joined forming four-fold and eight-fold rings. The tetrahedral sheets are linked directly to the

56 octahedral sheets to assemble a typical layer structure. The eight-membered rings formed by
57 CuO_6 octahedra are elongated and oriented in the same direction as the eight-membered rings
58 formed by PO_4 and $ZnO_3(OH)$ tetrahedra. These eight-fold rings create channels along **a** the
59 walls of which are decorated by H_2O molecules. The H_2O molecules are loosely bonded to the
60 Cu^{2+} atoms. The long Cu-H_2O distances, between 2.34 and 2.62 Å, are due to the distorted
61 octahedral coordination according to the Jahn-Teller effect (Jahn and Teller 1937).
62 The mineral used in this study originates from Zdravo Vrelo, near Kreševo (Bosnia and
63 Herzegovina). At this locality, veszelyite occurs in baryte veins as isometric blue to dark
64 green crystals in association with tetrahedrite, pyrite, covellite, malachite and other minerals
65 (Janjić et al. 1973). The paragenesis belongs to low-temperature hydrothermal activities, in
66 which veszelyite was formed in the oxidation zone (Vulić et al. 2007). Veszelyite is regarded
67 a supergene mineral characteristic of Cu-Zn mining activity. The mineral was identified for
68 the first time in Morawitza, Romania (Zsivny 1932), and has also been reported from Hisaichi
69 (Arakawa) mine, Japan (Sadanaga and Bunno 1974) and Kamioka mine, Gifu-Prefecture,
70 Honshu, Japan (Sakurai et al. 1952); Kipushi, Zaire (Lhoest 1995); Kabwe, Zambia (formerly
71 Broken Hill in northern Rhodesia) (Zsivny 1932); Wanlockhead, Scotland (Green 1990);
72 Gold Hill mining district, Utah (El-Shatoury and Whelan 1970). The world's largest
73 veszeylite crystals of approximately 5 cm were discovered in the Black Pine mine 12
74 kilometers northwest of Philipsburg, Montana (Waisman 1992). In addition the mineral
75 occurs at the La Esperanza mine Zacapoaxtly district, Puebla, Mexico (Panczner 1987).
76 Veszeylite was used as blue-green Maya pigment on funerary paraphernalia, such as masks,
77 miniatures and vases found in Calakmul, Mexico (Moreno et al. 2008a).
78 The substitution of Zn at the octahedral sites varies from $(Cu_{1.91}Zn_{0.09})Zn(PO_4)(OH)_3 \cdot H_2O$
79 at Arakawa mine Japan (Zsivny, 1932) to $(Cu_{1.47}Zn_{0.53})Zn(PO_4)(OH)_3 \cdot H_2O$ at Kamioka mine,
80 Japan (Harada 1954).

Originally motivated by the similarity of the complex PO_4-$ZnO_3(OH)$ sheet in veszelyite with topologically identical sheets of SiO_4 tetrahedra in cavansite (Danisi et al. 2012) and SiO_4 - AlO_4 tetrahedra in gismondine or amicite (Fischer 1963; Alberti and Vezzalini 1979), the purpose of this study is to determine the hydrogen-bond system and to understand the dehydration behavior of veszelyite. The H_2O molecules in veszelyite located in the eight-membered rings appear at first glance to be somewhat zeolitic in character. Thus, the knowledge of the structural modifications induced by heating is a first attempt in understanding the flexibility and stability of the layer structure of veszeylite.

2. EXPERIMENTAL METHODS

Single-Crystal X-ray diffraction

The chemical composition of veszelyite from Zdravo Vrelo was determined by electron microprobe analysis (Vulić et al. 2007) as $(Cu_{1.76}Zn_{0.24})_2Zn(PO_4)(OH_3)\cdot 2H_2O$.

A veszelyite single crystal from Zdravo Vrelo, near Kreševo (Bosnia and Herzegovina) of approximate dimensions 0.1 × 0.1 × 0.2 mm was selected for structure study and mounted in an open 0.1 mm diameter quartz-glass capillary. Single-crystal X-ray diffraction data were collected with a Bruker APEX II SMART diffractometer using Mo*K*α (λ = 0.71073 Å) X-ray radiation with 50 kV and 30 mA X-ray power. In order to study in situ dehydration, complete data sets were collected in steps of 25 °C up to 225 °C using a self-constructed temperature controlled hot nitrogen blower. Before data collections the crystal was kept at least 30 min at the next measuring temperature.

CCD area-detector data were integrated and an empirical absorption correction was applied using the Apex2 v. 2011.4-1 software package (Bruker 2011). Data-collection parameters and refinement parameters are given in Table 1. Neutral atom scattering-factors were used for structure refinement with SHELXL-97 (Sheldrick 2008). Hydrogen positions were extracted from difference-Fourier maps and refined with fixed isotropic displacement

parameters applying the restraints H-O = 0.95(1) Å and H-H = 1.59(5) Å. The hydrogen sites were located in refinements up to 125 °C. The experimentally derived hydrogen-bond system was confirmed by using bond-valence calculations (Brown and Altermatt 1985).

Initial atomic labels were those of Ghose et al. (1974) but the standard space-group setting $P2_1/c$ was chosen in contrast to $P2_1/a$ preferred by Ghose et al. (1974) requiring interchange of **a** and **c**. The final refinement, including hydrogen positions, for the data collected at room temperature, based on 2191 observed reflections and 140 parameters with 9 restraints, converged at R1 = 0.0187. Refinements for the data collected at 200 °C converged at R1 = 0.0716. The poor refinement reported at 200 °C (Table 1) is due to the transformation of veszeylite into a new phase characterized by the shortening of the **b** axis, the stretching of the **c** axis and poor quality of the diffraction pattern consisting of smeared reflections. The transformation into a new phase started at 150 °C with an extremely poor diffraction pattern. We decided to report the 200 °C diffraction data which allowed a better refinement.

Single crystal data at the temperature of -100 °C were collected with a Stoe IPDS2 imaging plate diffractometer equipped with Oxford Cryostream (University of Innsbruck) using MoKα (λ = 0.71073 Å) X-ray radiation with 50 kV and 40 mA power. The detector - sample distance was 100 mm and exposure time 15 min./frame. An analytical absorption correction based on 21 indexed faces was applied. The observed reflections were indexed with monoclinic unit cell in $P2_1/c$: a = 7.4863(4), b = 10.1933(4), c = 9.7895(4) Å, β = 103.180(4)°, V = 727.36 Å^3. Data were processed by Stoe X-Area software (Stoe and Cie 2007). Refinements for the data collected at -100 °C converged at R1 = 0.0263.

In order to provide a quantitative estimate for the distortion of the structure at different temperatures we calculate the L/S ratio (Bauer and Baur 1998). This ratio is measured between opposite oxygen sites along the shortest (S) and longest (L) cross-sections of the eight-membered rings of the octahedral and the tetrahedral sheets.

TG/DTA analysis

TG/DTA was conducted at the Department of Chemistry and Biochemistry, University of Bern, with a Mettler Toledo TGA/SDTA851 instrument using a sample from Zdravo Vrelo, Bosnia and Herzegovina. The sample of 11.28 mg was ground to a fine powder and placed into a 70 μL alox crucible. Between 25 and 600 °C a heating rate of 5 °C/min was used with a gas flow rate of 20 mL/min. The analysis was conducted under a dry helium atmosphere.

Raman spectroscopy

Confocal Raman spectra of single crystals were obtained with a HORIBA JOBIN YVON LabRam-HR 800 Raman micro-spectrometer. The sample was excited by the 515 nm emission line of a 100 mW Ar^{+}-laser under an OLYMPUS 100 X objective (N.A. = 0.9). The size and power of the laser spot on the surface were approximately 1 μm and 5 mW, respectively. The scattered light was dispersed by a grating with 1800 lines/mm and collected by a 1024 X 256 open electrode CCD detector. The spectral resolution, determined by measuring the Rayleigh line, was about 1.4 cm^{-1}. Third order polynomial and convoluted Gauss-Lorentz functions were applied for background correction and band fitting. The wavenumber accuracy of about 0.5 cm^{-1} was achieved by adjusting the zero-order position of the grating and regularly checked by a neon spectral calibration lamp.

3. RESULTS

Atomic coordinates and displacement parameters for the veszelyite structure at room temperature and 200 °C are given in Tables 2 and 3, respectively. The atomic coordinates and displacement parameter at -100 °C are reported in Table 4 (deposited). Selected distances and angles of hydrogen bonds under ambient conditions and at 200 °C are in Table 5.

Table 6 (deposited) compares the interatomic distances at room temperature and 200 °C. Results of bond valence calculations for veszelyite at room temperature and 200 °C are reported in Table 7 (deposited). Observed Raman bands (cm^{-1}) and possible assignments in

158 the spectrum of veszelyite at ambient conditions are indicated in Table 8. Table 9 (deposited)
159 lists the L/S ratios of the longest to the shortest cross-sections of eight-membered rings of
160 veszelyite at different temperature.
161

162 ## 4. DISCUSSION

163 *4.1. The structure of veszelyite under ambient conditions*

164 The structural study under ambient conditions confirmed that veszelyite is built by
165 alternating tetrahedral and octahedral sheets (Figs. 1-2) in agreement with the results by
166 Ghose et al. (1974), Berry (1948) and Vulić et al. (2007).

167 The H positions were determined from -100 °C up to 125 °C without substantial change in
168 the related hydrogen bonding scheme (Fig. 1). Bond-valence calculations (Brown and
169 Altermatt 1985) were used to corroborate the experimentally derived hydrogen-bond system.
170 Ignoring the contribution of hydrogen bonds in the bond valence sums (bvs) of oxygen atoms,
171 a bvs < 0.5 valence units (vu) indicates a H_2O molecule while a bvs of about 1 vu is typical of
172 OH groups. Moreover, a bvs below 2 vu but greater than 1.5 vu suggests that the oxygen atom
173 could be an acceptor of a hydrogen bond. As reported in Table 7a, OH1, OH2 and OH3 have
174 a bvs of about 1 vu characteristic of OH groups while H_2O1 and H_2O2 have bvs < 0.5 vu
175 indicating H_2O molecules. In addition, O1, O2, O3 and O4 show low bvs and participate at
176 hydrogen bonds as acceptors. The bvs for a donor of a hydrogen bond was increased by ca.
177 0.8 vu and the bvs of an acceptor by ca. 0.2, in accordance with the model by Ferraris and
178 Ivaldi (1988).

179 The seven located H positions indicate that there are five strong hydrogen bonds (Table 5)
180 with H···O acceptor distances below 2.0 Å: OH1-H1···H_2O1, OH2-H2···O2, OH3-H3···O1,
181 H_2O1-H5···OH2, H_2O2-H7···O4. The H_2O1-H4···O2 and H_2O2-H6···O3 interactions are weak
182 and the corresponding H···O acceptor distance is between 2.07 and 2.45 Å with d(H_2O1···O2) =

183 3.373(2) Å and d($H_2O2^{\cdots}O3$) = 2.8958(19) Å. The hydrogen-bond system links the tetrahedral
184 sheet to the octahedral sheet and also interconnects the Cu sheet (Fig. 3a). The hydrogen bond
185 system delineated in this study is only in partial agreement to that reported by Ghose et al.
186 (1974). In particular, OH1 interpreted (Ghose et al. 1974) as virtually free of hydrogen bond
187 is here characterized by a strong $OH1^{\cdots}H_2O1$ interaction (Table 5) and the corresponding
188 angle between donor-hydrogen-acceptor (DHA) is 166(4)°. Moreover, the oxygen at the
189 H_2O1 site acts as acceptor and donor of hydrogen bonds (Table 5).

190 The O-H stretching region in the wavelength range 4000 to 3000 cm^{-1} of the IR spectrum
191 of veszelyite is characterized by two peaks at 3530 (sharp), 3270 (broad) cm^{-1}, with two
192 shoulders at 3350 cm^{-1} and 3170 cm^{-1} (Ghose at al. 1974). According to the hydrogen bond-
193 length versus IR frequency correlation by Libowitzky (1999) absorptions between 3270 and
194 3530 cm^{-1} correspond to donor-acceptor ($O^{\cdots}O$) distances of ca. 2.73 – 2.93 Å, which agrees
195 with the D-A distances in Table 5. The two strong hydrogen bonds H_2O1-$H5^{\cdots}OH2$ and H_2O2-
196 $H7^{\cdots}O4$ with D-A distances of about 2.6 Å should show absorption peaks at ca. 2730 cm^{-1}, not
197 observed in the IR spectrum reported by Ghose et al. (1974). However, two broad bands at
198 2664 and 2852 cm^{-1} besides 8 further bands between 3184 and 3555 cm^{-1} were observed in the
199 Raman spectrum collected on Zdravo Vrelo veszelyite shown in Fig. 4. The large number of
200 bands in this region can be assigned to stretching vibrations of hydroxyl and H_2O units and
201 are consistent with the complex hydrogen bond system.

202 The Raman spectrum of veszelyite below 2500 cm^{-1} matches with the spectra presented in
203 Moreno et al. (2008b). It is characterized by the most intense band (amplitude) at 967 cm^{-1},
204 medium intensity bands at 624, 486, 470 387, 377, 364, 243 and 130 cm^{-1} and numerous
205 weaker bands (Table 8). Scattering measurements on phosphates in aqueous solutions
206 (Nakamoto 1978), Zn phosphate minerals (Frost 2004) and *ab initio* studies of hydroxyapatite
207 (Corno et al. 2006) assign the Raman bands in water-bearing phosphates to ν_3 asymmetric P-O
208 stretching modes ~1020-1095 cm^{-1}, ν_1 symmetric P-O stretching modes around 950-990 cm^{-1},

209 ν_4 asymmetric OPO bending ~ 530-660 cm^{-1}, ν_2 symmetric OPO bending modes ~ 400-490
210 cm^{-1} and complex lattice modes involving Zn-O and Cu-O vibrations < 400 cm^{-1}.

211 The origin of the additional bands at 833 and 882 cm^{-1} and from 1379-2233 cm^{-1} is
212 unclear. Compared to other zinc and zinc calcium phosphates the symmetry of veszelyite is
213 lower and the structure more complex, resulting in a higher number of theoretical possible
214 vibrational modes. Further explanations might be vibrational overtones caused by second
215 order Raman scattering processes or vibrational modes of H_2O and OH groups. The existence
216 of translational modes of OH groups at 335 and 630 cm^{-1} was reported for hydroxyapatite
217 (Corno et al. 2006 and references therein).

218

219 *4.2. Dehydration upon heating*

220 The observed dehydration beginning at 150 °C is preceded by a slight increase of volume
221 due to thermal expansion. This dehydration step is associated with complete loss of H_2O at
222 the H_2O2 site. After release of H_2O2 the Cu coordination of Cu1 and Cu2 declined from
223 originally six- to five-fold. Cu is no longer in distorted octahedral coordination but occupies a
224 distorted square-based pyramid (Fig. 5). H_2O1 moves towards a position in the center of the
225 eight membered rings (Figs. 1-2). Moreover, the Cu2-H_2O1 distance decreased from
226 2.4441(16) to 2.248(10) Å. Simultaneously to the water loss, the unit-cell volume decreased
227 by 7% from originally 734.45(3) $Å^3$ to 686.4(4) $Å^3$ leading to a formula with 1 H_2O pfu (Fig.
228 6). The new phase observed above 150 °C is characterized by increase of the **c** axis and
229 shortening of the **b** axis (Table 1). The expansion of the **c** axis is related to strain relaxation
230 within the four- and eight-membered rings and to the deformation imposed by the distortion
231 of the T-O-T angles. This T-O-T bending causes distortion of the tetrahedral and octahedral
232 sheets (Fig. 2). The L/S ratio of the eight-membered rings of the tetrahedral sheet and the
233 octahedral sheet increases between room temperature and 200 °C yielding more pronounced
234 elliptical shape of the channels with dehydration (Table 9). Moreover, the bases of the

tetrahedra forming sheets parallel to (100) describe a puckered surface as result of the strain relaxation within the eight-membered rings (Fig. 2). In contrast, at room temperature the bases of tetrahedra form flat layers (Fig. 1). The deformations of the tetrahedral sheets are monitored by variations of T-O-T angles at different temperature (Table 6). The P-O1-Zn and P-O2-Zn angles increased from 132.42° and 120.59° at room temperature to 135.6° and 123.1° at 200 °C, respectively. The P-O4-Zn angle decreased from 131.23° to 127.5°.

The deformation of the framework imposed by the release of water implies a rearrangement of the hydrogen-bond system (Fig. 3b). The poor data quality and refinement at 200 °C did not allow determination of the H positions. The evaluation of the hydrogen-bond system at 200 °C is based on bond-valence calculations (Brown and Altermatt 1985) and donor-acceptor distances (Table 5b). As reported in Table 7b, the increased bond valence sum (without hydrogen bond contributions) at O4 is due to the shortening of the P-O4 distance. O4 at 200 °C is no longer fixed by a hydrogen bond, which is in contrast to our structural data below 150 °C. The bonds OH2-H2···O2 and OH3-H3···O1 are preserved at 200 °C (Table 5). The H_2O1 site rearranges the hydrogen bonds generating two new interactions: H_2O1-H4···O3 and H_2O1-H5···O2. The strong interaction H_2O1-H5···OH2 with D-A distance 2.63 Å at room temperature is no more observed. The D-A distance H_2O1···O2 shortens from 3.37 Å at room temperature to 2.87 Å at 200 °C. The OH1 site generates a new hydrogen bond to OH2 with a D-A distance of 2.96 Å. As observed at room temperature, the hydrogen-bond system at 200 °C strengthens the connection between the tetrahedral and the octahedral sheet (Fig. 3b).

Already at 125 °C (before release of H_2O2) O4 shows increased anisotropy in thermal motion parallel to **a** and perpendicular to the P-O4-Zn connection. This behavior is depicted in Fig. 7 in terms of temperature dependence of U_{eq}. At first glance it appears surprising that H_2O2, which is expelled first, has lower U_{eq} than H_2O1. This is explained by two bonds of H_2O2 to Cu1 and Cu2 whereas H_2O1 is only bonded to Cu2. Above 125 °C O4 shows the strongest thermal disorder (Figs. 7 and 8) comparable to H_2O1. The sites from O1 to O3 and

the oxygen atoms of the hydroxyl groups show the same behavior with a slight increase of the U_{eq} after 125 °C.

Our dehydration experiments were carried out up to 225 °C. At this temperature we observed that the color changed from blue to green accompanied by breakdown of the partially dehydrated structure. With removal of the last H_2O molecule at H_2O1, the crystal structure collapsed. At first glance we would have expected that after the release of H_2O at H_2O1 Cu adopted square planar 4-fold coordination preserving the crystal structure. Loss of H_2O1 would not lead to unreasonable bond valence sums for oxygen or Cu (Table 7b).

Few natural examples of crystal structures with Cu^{2+} in planar fourfold-coordination are reported in the literature: elyite $Pb_4Cu(SO_4)O_2(OH)_4 \cdot H_2O$ (Kolitsch and Giester 2000), johillerite $Na(Mg,Zn)_3Cu(AsO_4)_3$ (Tait and Hawthorne 2004), henmilite $Ca_2Cu(OH)_4[B(OH)_4]_2$ (Nakai et al. 1986) and cuprorivaite $CaCuSi_4O_{10}$ (Bensch and Schur 1995).

However, a crystalline anhydrous veszelyite phase was not observed and the reason is attributed to the substitution of Cu by Zn in the octahedral sheet. As the Cu2 octahedron is less distorted than Cu1, Zn substitution is more probable for Cu2. Looking at the probability ellipsoids in Figure 5, there is no clear indication of preferential occupancy of Zn at Cu1 or Cu2. We would expect that a Jahn-Teller distorted octahedron with mixed Zn, Cu occupancy shows smeared probability ellipsoids along the Jahn-Teller active ligands. The problem of Zn preference for different Cu sites in veszelyite and other structures is addressed by Mellini and Merlino (1978). On the base of the different octahedral distortions of the two sites, they assume that Cu1 is fully occupied by Cu whereas Cu2 is partially substituted by Zn. The ΔL value (difference between the average values of axial and equatorial bond distance) for Cu1 indicates 100% Cu content. This hypothesis supports the idea that if H_2O at H_2O1 is released Zn cannot adopt planar four-fold coordination and for this reason the breakdown of the structure occurs.

The weight loss between 130 and 220 °C seen in our thermo-gravimetric analysis (Fig. 9 deposited) correlates with the transitions at 150 °C in our study. The second step between 220 and 290 °C is related to the loss of the last H_2O molecule at the H_2O1 site. The last step (290-600 °C) corresponds to the loss of OH groups. The total mass lost during the 25 to 600 °C heating excursion sums up to 17.5 wt% (Fig. 9).

4.4. Similarities and differences between veszelyite and related structures

The veszelyite structure has some similarity to that of the zeolite-like cavansite framework ($Ca(VO)Si_4O_{10}\cdot 4H_2O$) (Evans 1973) and gismondine ($CaAl_2Si_2O_8\cdot 4H_2O$) (Vezzalini et al. 1993). These structures have tetrahedral sheets composed of four- and eight-membered rings in common with the same up and down arrangement of tetrahedral apices in adjacent chains.

In cavansite the dehydration proceeds in four steps within the same space group with only minor impact on framework distortion and contraction (Danisi et al. 2012). The removal of the last H_2O molecule causes structural destruction in both structures. In particular, the lowest coordination limit for the cations (Cu or Ca) bonded to the H_2O molecules appears to be five. In veszelyite Zn substituted Cu2 cannot adopt square planar four-fold coordination while Ca in cavansite, after losing the last H_2O molecule, cannot preserve the five-fold coordination thus causing structural breakdown.

An interesting analogy could be drawn between veszelyite and kipushite. In both structures the sheet composed by alternating PO_4 and $ZnO_3(OH)$ tetrahedra is very similar (Piret et al. 1985). The kipushite structure is also built of sheet of ZnO_4 and PO_4 tetrahedra neighbored by two octahedral sheets like in veszelyite but each second tetrahedral sheet is replaced by isolated PO_4 tetrahedra. In both structures, Zn fully occupies a tetrahedral site and partially substitutes Cu in octahedral coordination. The up and down arrangement of tetrahedral apices in adjacent chains in veszelyite corresponds to the arrangement in kipushite.

Tetrahedral sheets composed by four- and eight- membered rings have been reported also for the layered hydrous zinc phosphate $Mg[ZnPO_4(H_2O)]_2 \cdot 10H_2O$ (Kahlenberg et al. 2008). The building units are PO_4 and $ZnO_3(H_2O)$ but in contrast to veszelyite the up and down arrangement of tetrahedral apices in adjacent chains is different.

A comparable open eight-membered octahedral sheet structure has been found in bayldonite (Ghose and Wan 1979). The $Cu^{2+}O_6$ octahedra show the usual Jahn-Teller distortion and Zn partially substitutes copper in octahedral coordination. As in veszelyite the Cu2 site appears to be the most probable site for Zn substitution.

ACKNOWLEDGEMENTS

Authors are deeply grateful D. Djordjević for supplying us a sample of veszelyite from Zdravo Vrelo (Bosnia and Herzegovina) for studying the dehydration behavior. The constructive reviews of Stefano Merlino and Reinhard X. Fischer are highly appreciated.

REFERENCES

Alberti, A. and Vezzalini, G. (1979) The crystal structure of amicite, a zeolite. Acta Crystallographica, B35, 2866-2869.

Bauer, T. and Baur, W.H. (1998) Structural changes in the natural zeolite gismondine (GIS) induced by cation exchange with Ag, Cs, Ba, Li Na, K and Rb. Europen Journal of Mineralogy, 10, 133-147.

Bensch, W. and Schur, M. (1995) Crystal structure of calcium copper phyllodecaoxotetrasilicate, $CaCuSi_4O_{10}$. Zeitschrift für Kristallographie, 210, 530.

Berry, L.G. (1948) Structural crystallography of lazulite, scorzalite and veszelyite. American Mineralogist, 33, 750.

Brown, I.D. and Altermatt, D. (1985) Bond-valence parameters obtained from a systematic analysis of the Inorganic Crystal Structure Database. Acta Crystallographica, B41, 244-247.

Bruker. (2011). SAINT, SADABS. Bruker AXS Inc., Medison, Wisconsin, USA.

Corno, M., Busco, C., Civalleri, B. and Ugliengo, P. (2006) Periodic ab initio study of structural and vibrational features of hexagonal hydroxyapatite $Ca_{10}(PO_4)_6(OH)_2$. Physical Chemistry Chemical Physics, 8, 2464-2472.

Danisi, R.M., Armbruster, T. and Lazic, B. (2012) In situ dehydration behavior of zeolite-like cavansite: a single crystal X-ray study. American Mineralogist, 97, 1874-1880.

El-Shatoury, H.M. and Whelan, J.A. (1970) Mineralization in the gold hill mining district, Tooele County, Utah. Utah Geological and Mineralogical Survey, Bulletin 83, 1-37.

Evans, H.T. Jr. (1973) The crystal structures of cavansite and pentagonite. American Mineralogist, 58, 412–424.

Ferraris, G. and Ivaldi, G. (1988) Bond valences vs bond length in O…O hydrogen bonds. Acta Crystallographica, B44, 341–344.

Fischer, K.F. (1963) The crystal structure determination of zeolite gismondite $CaAl_2Si_2O_8{\cdot}4H_2O$. American Mineralogist, 48, 664-672.

Frost, R.L. (2004) An infrared and Raman spectroscopic study of natural zinc phosphates. Spectrochimica Acta. Part A, Molecular and Biomolecular Spectroscopy 60, 1439-1445.

Ghose, S., Leo, S.R. and Wan, C. (1974) Structural chemistry of copper and zinc minerals. Part I. Veszelyite, $(Cu,Zn)_2Zn(PO_4)(OH)_3{\cdot}2H_2O$: a novel type of sheet structure and crystal chemistry of copper-zinc substitution. American Mineralogist, 59, 573-581.

Ghose, S. and Wan, C. (1979) Structural Chemistry of copper and zinc minerals VI. Bayldonite, $(Cu,Zn)_3Pb(AsO_4)_2(OH)_2$: a complex layer structure. Acta Crystallographica, B35, 819-823.

Green, D. (1990) Veszelyite a mineral new to Britain, from Wanlockhead, Scotland. Journal of Mines and Minerals, 8, 6-7.

Harada, Z. (1954) Chemical Analyses of Japanese Minerals (III). Journal of the Faculty of Science, Hokkaido University. Series 4, Geology and Mineralogy, 8(4), 289-348.

Jahn, H.A. and Teller, E. (1937). Stability of polyatomic molecules in degenerate electronic States. I. Orbital Degeneracy. Proceedings of the Royal Society of London. Series A, Mathematical and Physical Sciences, 161, 220-235.

Janjić, S., Đorđević, D., Jovanović, R. and Bugarski, P. (1973) Pojava vescelita (veszelyita) u području Kreševa (Jugoslavija). Geološki Glasnik, 17, 181-192.

Kahlenberg, V., Tessadri, R., Többens, D.M., Wertl, W. and Rössler, A. (2008) $Mg[ZnPO_4(H_2O)]_2 \cdot 10H_2O$ – a layered hydrous zinc phosphate retrieved from an industrial filter cake residual, Zeitschrift für Anorganische und Allgemeine Chemie, 634, 1181-1186.

Kolitsch, U. and Giester, G. (2000) Elyite, $Pb_4Cu(SO_4)O_2(OH)_4 \cdot H_2O$: Crystal structure and new data. American Mineralogist, 85, 1816-1821.

Libowitzky, E. (1999) Correlation of O-H stretching frequencies and O-H hydrogen bond lenghts in minerals. Monatshefte für Chemie, 130, 1047–1059.

Lhoest, J.J. (1995) The Kipushi Mine. Mineralogical Record, 26, 163-192.

Mellini, M. and Merlino, S. (1978) Ktenasite, another mineral with $[(Cu,Zn)_2(OH)_3O]^-$ octahedral sheets. Zeitschrift für Kristallographie, 147, 129-140.

Moreno, R.G., Mathis, F., Mazel ,V., Dubus, M., Calligaro, T. and Strivay, D. (2008a) Discovery and characterization of an unknown blue-green Maya pigment: veszelyite. Archaeometry, 50, 658-667.

Moreno, R.G., Strivay, D. and Gilbert, B. (2008b) Maya blue-green pigments found in Calakmul, Mexico: a study by Raman and UV-visible spectroscopy. Journal of Raman spectroscopy, 39, 1050-1056.

Nakai, I., Okada, H., Masutomi, K., Koyama, E. and Nagashima, K. (1986) Henmilite, $Ca_2Cu(OH)_4[B(OH)_4]_2$, a new mineral from Fuka, Okayama Prefecture, Japan. American Mineralogist, 71, 1234–1239.

Nakamoto, K. (1978) Infrared and Raman spectra of inorganic and coordination compounds, Wiley, New York, 448 p.

Panczner, W. D. (1987) Minerals of Mexico: New York, Van Nostrand Reinhold Company, 459 p.

Piret, P., Deliens, M. and Piret-Meunier, J. (1985) Occurrence and crystal structure of kipushite, a new copper-zinc phosphate from Kipushi, Zaire. Canadian Mineralogist, 23, 35-42.

Sadanaga, R. and Bunno, M. (1974) The Wakabayashi mineral collection. The University museum, the University of Tokio Bulletin no. 7, 177 p.

Sakurai, K, Nagashima, H. and Sorita, E. (1952) Kamiokalite, a new zinc copper phosphate mineral from Kamioka Mine, Japan. Syumi-no-Tigaku (Amateur Geologist), 5, 170-175.

Sheldrick G.M. (2008) A short history of SHELX. Acta Crystallographica A64, 112-122.

417 Stoe and Cie, 2007. X-Area 1.39. Darmstadt, Germany.

418 Tait, K.T. and Hawthorne, F.C. (2004) Johillerite from Tolbachik, Kamchatka Peninsula,
419 Russia: crystal-structure refinement and chemical composition. Canadian Mineralogist 42,
420 717-722.
421
422 Vezzalini, G., Quartieri, S. and Alberti, A. (1993) Structural modifications induced by
423 dehydration in the zeolite gismondine. Zeolites, 13, 34–42.

424 Vulić P., Kahlenberg, V., Lazic, B., Kaindl, R., Dimitrijević, R. and Djordjević, D. (2007)
425 Veszelyte from the locality Zdravo Vrelo near Kreševo (Bosnia and Herzegovina): its
426 mineralogical characterization and absolute crystal structure. XIV Conference of the Serbian
427 Crystallographic Society (28-30 June 2007) Vršac, Serbia, the Book of Abstracts, pp. 16-17.

428 Waisman, D. (1992) Minerals of the Black Pine Mine, Granite county, Montana.
429 Mineralogical Record, 23, 477-483.

430 Zsivny, V. (1932) Ueber den Veszelyit von Vaskö (Moravicza). Zeitschrift für
431 Kristallographie, 82, 87-110.
432

FIGURE CAPTIONS

Figure 1. Structure of veszelyite at room temperature. The green tetrahedra represent Zn, while PO_4 tetrahedra are yellow. Octahedra around Cu2 are light blue and octahedra around Cu1 are dark blue. H_2O molecules are shown as pink spheres with attached small white spheres representing H. Hydrogen-bond acceptor interactions are shown by gray dashed connectors. (a) Projection along the **b** axis showing the tetrahedral and octahedral sheets, (b) view of the veszelyite structure parallel to **a** showing the four- and eight-member rings of tetrahedra overlapping the eight-member rings of octahedra.

Figure 2. Structure of veszelyite at 200 °C. (a) Projection along the **b** axis, (b) View of the veszelyite structure parallel to **a**. Colors as in Fig. 1.

Figure 3. Hydrogen-bond system of veszelyite. (a) Hydrogen bonding at RT. H_2O molecules are shown as pink spheres and the numbers 1 and 2 refer to H_2O1 and H_2O2 sites, respectively. (b) Hydrogen bonding at 200 °C, the black arrows indicate the direction to the acceptor. Colors as in Fig. 1.

Figure 4. Deconvolution of the Raman spectrum of veszelyite in the range 2500 – 4000 cm^{-1}. Dots – measured Raman spectrum, thin curves – fitted Gauss-Lorentz functions, thick curve – sum curve of fitted functions..

Figure 5: Displacement ellipsoids for Cu1 and Cu2 polyhedra in veszelyite at RT and 200 °C. The probability for ellipsoids is 0.75.

Figure 6. Development of unit-cell volume versus temperature for in situ dehydration experiments of veszelyite. The size of the symbols is larger than the associated esd's.

Figure 7. U_{eq} for oxygen sites at different temperatures for veszelyite. The size of the symbols is larger than the associated esd's

Figure 8: Thermal ellipsoids for P and Zn polyhedra in veszelyite at RT and 200 °C. The probability for ellipsoids is 0.75.

Figure 9: Weight curve and calculated mass loss of veszelyite.

Table 1. Parameters for X-ray data collection and crystal-structure refinement of veszelyite.

Crystal data	*Veszelyite* (RT)	*Veszelyite* (200 °C)
Unit cell dimensions (Å)	a = 7.5096(2)	a = 7.252(4)
	b = 10.2281(2)	b = 9.233(5)
	c = 9.8258(2)	c = 10.520(5)
	β = 103.3040(10)	β = 102.076(15)
Volume (Å^3)	734.45(3)	688.8(6)
Space group	$P2_1/c$ (No. 14)	$P2_1/c$ (No. 14)
Z	4	4
Chemical formula	$(Cu_{1.76}Zn_{0.24})_2Zn(PO_4)(OH_3)\cdot 2H_2O$	$(Cu_{1.76}Zn_{0.24})_2Zn(PO_4)(OH_3)\cdot 1H_2O$
Intensity measurement		
Crystal shape	prismatic	prismatic
Crystal size (mm)	0.1 × 0.1 × 0.2	0.1 × 0.1 × 0.2
Diffractometer	APEX II SMART	APEX II SMART
X-ray radiation	Mo$K\alpha$ λ = 0.71073 Å	Mo$K\alpha$ λ = 0.71073 Å
X-ray power	50 kV, 30 mA	50 kV, 30 mA
Monochromator	graphite	graphite
Temperature	296 K	473 K
Time per frame	30 sec	30 sec
Max. θ	33.66	27.92
Index ranges	$-10 \le h \le 11$	$-7 \le h \le 9$
	$-14 \le k \le 15$	$-11 \le k \le 12$
	$-13 \le l \le 12$	$-12 \le l \le 12$
No. of measured reflections	8010	4483
No. of unique reflections	2431	1575
No. of observed reflections ($I > 2\sigma(I)$)	2191	922
Refinement of the structure		
No. of parameters used in refinement	140 + 9 restraints *	111
R_{int}	0.0248	0.1027
R_σ	0.0268	0.1190
$R1$, $I > 2\sigma(I)$	0.0187	0.0716
$R1$, all data	0.0222	0.1315
w$R2$ (on F^2)	0.0494	0.1930
GooF	0.982	1.036
$\Delta\rho_{min}$ (-e / Å^3)	-0.54 close to Cu1	-1.72 close to Cu2
$\Delta\rho_{max}$ (e / Å^3)	0.58 close to O3	1.89 close to OH1

* Hydrogen positions refined.

Table 2a. Atomic coordinates and U_{eq} (U_{iso}) (Å^2) values for veszelyite at RT.

Site	*Atom*	*Occ.*	x	y	z	U_{eq}/U_{iso}
Cu1	Cu	1	0.49119(3)	0.073201(19)	0.12977(2)	0.01159(6)
Cu2	Cu,Zn[1)]	1	0.46075(3)	0.25309(2)	0.35875(2)	0.01117(6)
Zn	Zn	1	0.06969(3)	0.076074(18)	0.21045(2)	0.01146(6)
P	P	1	0.06592(6)	0.29887(4)	0.41457(5)	0.00931(9)
O1	O	1	0.97533(18)	0.15924(13)	0.03207(13)	0.0152(3)
O2	O	1	0.98311(17)	0.16643(12)	0.35793(13)	0.0138(3)
O3	O	1	0.27509(17)	0.28533(12)	0.46986(13)	0.0128(2)
O4	O	1	0.0246(2)	0.40001(12)	0.29562(15)	0.0161(3)
OH1	O	1	0.33809(18)	0.08578(11)	0.26875(14)	0.0119(2)
H1	H	1	0.359(5)	0.023(3)	0.340(3)	0.080*
OH2	O	1	0.62201(17)	0.21779(12)	0.23336(14)	0.0128(2)
H2	H	1	0.740(2)	0.190(3)	0.280(3)	0.080*
OH3	O	1	0.59993(17)	0.40805(11)	0.46354(14)	0.0112(2)
H3	H	1	0.7248(19)	0.386(4)	0.488(4)	0.080*
H_2O1	O	1	0.6558(2)	0.38343(15)	0.03669(16)	0.0252(3)
H4	H	1	0.760(3)	0.370(4)	0.001(4)	0.080*
H5	H	1	0.656(5)	0.334(3)	0.117(2)	0.080*
H_2O2	O	1	0.3199(2)	0.40648(15)	0.19194(17)	0.0238(3)
H6	H	1	0.323(5)	0.374(4)	0.103(2)	0.080*
H7	H	1	0.202(3)	0.402(3)	0.209(4)	0.080*

* U_{iso} of hydrogen was fixed.

[1)] See Discussion

Table 2b. Atomic coordinates and U_{eq} (Å^2) values for veszelyite at 200 °C.

Site	*Atom*	*Occ.*	x	y	z	U_{eq}
Cu1	Cu	1	0.4798(2)	0.08719(14)	0.11512(13)	0.0290(4)
Cu2	Cu,Zn[1)]	1	0.4742(2)	0.22291(15)	0.36711(14)	0.0315(5)
Zn1	Zn	1	0.0541(2)	0.07741(14)	0.19716(14)	0.0317(5)
P4	P	1	0.0902(5)	0.2150(3)	-0.0771(3)	0.0282(8)
O1	O	1	-0.0130(12)	0.1742(9)	0.0301(8)	0.035(2)
O2	O	1	-0.0201(12)	0.1634(10)	0.3432(8)	0.038(2)
O3	O	1	0.2947(12)	0.2645(8)	-0.0172(8)	0.0302(19)
O4	O	1	-0.1070(15)	-0.0902(9)	0.1639(10)	0.051(3)
OH1	O	1	0.3324(13)	0.0610(8)	0.2501(8)	0.034(2)
OH2	O	1	0.6023(13)	0.2449(8)	0.2223(9)	0.037(2)
OH3	O	1	0.6005(11)	0.1039(7)	-0.0372(8)	0.0282(18)
H_2O1	O	1	0.6902(17)	0.0653(11)	0.4712(13)	0.067(5)

[1)] See Discussion.

Tables 3a-3b for deposit

Table 3a. Anisotropic displacement parameters (Å^2) for veszelyite at RT.

Site	U_{11}	U_{22}	U_{33}	U_{23}	U_{13}	U_{12}
Cu1	0.01235(11)	0.01255(10)	0.01121(12)	-0.00326(7)	0.00543(8)	-0.00264(7)
Cu2	0.01099(11)	0.01187(10)	0.01168(12)	-0.00293(7)	0.00472(8)	-0.00128(7)
Zn	0.01111(10)	0.01221(9)	0.01126(12)	-0.00107(7)	0.00295(8)	-0.00146(6)
P	0.0084(2)	0.01001(17)	0.0099(2)	-0.00132(14)	0.00289(16)	0.00010(14)
O1	0.0129(6)	0.0211(6)	0.0130(7)	0.0051(5)	0.0059(5)	-0.0001(5)
O2	0.0125(6)	0.0129(5)	0.0167(7)	-0.0043(5)	0.0049(5)	-0.0018(4)
O3	0.0081(6)	0.0164(5)	0.0139(7)	-0.0021(5)	0.0024(5)	-0.0005(4)
O4	0.0195(7)	0.0140(5)	0.0164(7)	0.0035(5)	0.0071(6)	0.0056(5)
OH1	0.0105(6)	0.0131(5)	0.0124(7)	0.0008(4)	0.0032(5)	-0.0009(4)
OH2	0.0112(6)	0.0145(5)	0.0132(6)	-0.0020(5)	0.0039(5)	-0.0013(4)
OH3	0.0102(6)	0.0120(5)	0.0123(7)	0.0013(4)	0.0043(5)	0.0015(4)
H_2O1	0.0322(9)	0.0237(7)	0.0192(8)	0.0026(6)	0.0049(7)	0.0018(6)
H_2O2	0.0182(7)	0.0324(8)	0.0221(8)	-0.0024(6)	0.0075(6)	-0.0009(6)

Table 3b. Anisotropic displacement parameters (Å^2) for veszelyite at 200 °C.

Site	U_{11}	U_{22}	U_{33}	U_{23}	U_{13}	U_{12}
Cu1	0.0366(9)	0.0255(7)	0.0274(9)	-0.0030(5)	0.0125(7)	-0.0023(6)
Cu2	0.0373(10)	0.0261(7)	0.0335(10)	-0.0075(6)	0.0129(7)	-0.0041(6)
Zn1	0.0377(9)	0.0271(7)	0.0313(9)	-0.0030(5)	0.0095(7)	-0.0037(6)
P	0.0295(18)	0.0237(14)	0.0314(18)	0.0032(11)	0.0064(15)	-0.0041(12)
O1	0.036(5)	0.035(4)	0.035(5)	0.011(4)	0.009(4)	-0.001(4)
O2	0.033(5)	0.051(5)	0.038(5)	-0.017(4)	0.020(4)	-0.003(4)
O3	0.036(5)	0.029(4)	0.027(5)	0.004(3)	0.011(4)	-0.005(3)
O4	0.061(7)	0.041(5)	0.056(6)	-0.015(4)	0.022(6)	-0.022(5)
OH1	0.043(5)	0.026(4)	0.038(5)	-0.003(3)	0.021(4)	0.003(4)
OH2	0.040(6)	0.032(4)	0.041(5)	-0.001(4)	0.014(4)	-0.007(4)
OH3	0.031(5)	0.023(4)	0.033(5)	0.000(3)	0.013(4)	0.006(3)
H_2O1	0.062(8)	0.049(7)	0.091(10)	0.023(6)	0.019(7)	0.016(5)

Table 4a-4b-4c-4d (for deposit)

Table 4a. Atomic coordinates and U_{eq} (U_{iso}) (Å^2) values for veszelyite at -100 °C

Site	*Atom*	*Occ.*	*x*	*y*	*z*	U_{eq}/U_{iso}
Cu1	Cu	1	0.49198(5)	0.07238(3)	0.13093(4)	0.01162(11)
Cu2	Cu,Zn	1	0.46096(5)	0.25245(3)	0.35992(3)	0.01119(11)
Zn	Zn	1	0.06991(5)	0.07500(3)	0.21193(3)	0.01166(11)
P	P	1	0.06580(10)	0.29795(7)	0.41611(7)	0.01059(15)
O1	O	1	0.9742(3)	0.1587(2)	0.0333(2)	0.0143(4)
O2	O	1	0.9831(3)	0.1641(2)	0.3609(2)	0.0133(4)
O3	O	1	0.2755(3)	0.2848(2)	0.4716(2)	0.0128(4)
O4	O	1	0.0241(3)	0.3982(2)	0.2951(2)	0.0143(4)
OH1	O	1	0.3384(3)	0.0858(2)	0.2706(2)	0.0115(4)
H1	H	1	0.355(10)	0.025(5)	0.345(5)	0.080
OH2	O	1	0.6237(3)	0.2175(2)	0.2350(2)	0.0124(4)
H2	H	1	0.740(5)	0.183(6)	0.279(7)	0.080
OH3	O	1	0.6003(3)	0.40765(19)	0.4639(2)	0.0115(4)
H3	H	1	0.727(3)	0.387(7)	0.484(8)	0.080
H_2O1	O	1	0.6559(3)	0.3839(2)	0.0381(2)	0.0196(4)
H4	H	1	0.765(5)	0.374(7)	0.006(7)	0.080
H5	H	1	0.653(9)	0.324(5)	0.111(5)	0.080
H_2O2	O	1	0.3212(3)	0.4065(2)	0.1931(2)	0.0185(4)
H6	H	1	0.319(9)	0.365(6)	0.106(4)	0.080
H7	H	1	0.208(5)	0.398(7)	0.220(7)	0.080

Table 4b. Anisotropic displacement parameters (Å^2) for veszelyite at -100 °C.

Site	U_{11}	U_{22}	U_{33}	U_{23}	U_{13}	U_{12}
Cu1	0.01277(18)	0.01137(18)	0.01161(18)	-0.00213(11)	0.00465(13)	-0.00168(11)
Cu2	0.01179(18)	0.01072(18)	0.01177(17)	-0.00159(12)	0.00416(12)	-0.00092(11)
Zn	0.01218(17)	0.01132(18)	0.01164(17)	-0.00062(11)	0.00304(12)	-0.00075(11)
P	0.0110(3)	0.0099(3)	0.0111(3)	-0.0007(2)	0.0029(2)	-0.0001(2)
O1	0.0130(9)	0.0163(10)	0.0141(9)	0.0031(8)	0.0039(7)	0.0004(8)
O2	0.0147(9)	0.0119(9)	0.0143(9)	-0.0022(7)	0.0049(7)	-0.0004(7)
O3	0.0118(9)	0.0153(10)	0.0120(9)	-0.0019(7)	0.0039(7)	-0.0010(7)
O4	0.0170(10)	0.0114(9)	0.0151(9)	0.0011(8)	0.0046(7)	0.0034(8)
OH1	0.0111(9)	0.0125(9)	0.0110(9)	-0.0001(7)	0.0028(7)	-0.0007(7)
OH2	0.0118(9)	0.0132(9)	0.0125(9)	-0.0016(7)	0.0032(7)	-0.0010(7)
OH3	0.0131(9)	0.0109(9)	0.0113(9)	0.0007(7)	0.0047(7)	-0.0004(7)
H_2O1	0.0232(11)	0.0181(10)	0.0177(10)	0.0011(8)	0.0051(8)	0.0002(9)
H_2O2	0.0152(10)	0.0229(11)	0.0180(10)	-0.0005(8)	0.0048(8)	-0.0013(8)

This is a preprint, the final version is subject to change, of the American Mineralogist (MSA)
Cite as Authors (Year) Title. American Mineralogist, in press.
(DOI will not work until issue is live.) DOI: http://dx.doi.org/10.2138/am.2013.4465

Table 4c. Hydrogen bond distances (Å) and O-H···O angles (°). H positions were determined with the restraint O-H is 0.95(1) Å and H-H = 1.59(5) Å. D: donor; A: acceptor.

Species	D-H	H…A	D…A	<(DHA)	Hydrogen bond
OH	0.945(10)	1.85(2)	2.776(3)	167(6)	OH1-H1···H2O1
OH	0.946(10)	1.83(2)	2.747(3)	164(6)	OH2-H2···O2
OH	0.947(10)	1.863(12)	2.808(3)	176(7)	OH3-H3···O1
H_2O	0.947(10)	2.43(2)	3.345(3)	163(6)	H2O1-H4···O2
H_2O	0.948(10)	1.675(13)	2.619(3)	174(6)	H2O1-H5···OH2
H_2O	0.947(10)	1.99(3)	2.878(3)	155(6)	H2O2-H6···O3
H_2O	0.948(10)	1.701(16)	2.638(3)	169(6)	H2O2-H7···O4

Table 4d. Interatomic distances (Å) and T-O-T angles (°) of veszelyite at -100 °C.

Cu1 coordination	-100 °C
Cu1-OH2	1.934(2)
Cu1-OH3(2×)	1.966(2)
	1.995(2)
Cu1-OH1	1.982(2)
Cu1-O3	2.455(2)
Cu1-H_2O2	2.586(2)
Mean	2.153
Cu2 coordination	-100 °C
Cu2-OH2	1.946(2)
Cu2-O3	1.981(2)
Cu2-OH3	2.035(2)
Cu2-OH1	2.031(2)
Cu2- H_2O2	2.334(2)
Cu2-H_2O1	2.438(2)
Mean	2.128
Zn coordination	-100 °C
Zn-O1	1.931(2)
Zn-O4	1.931(2)
Zn-O2	1.951(2)
Zn-OH1	1.964(2)
Mean	1.944
P coordination	-100 °C
P-O1	1.530(2)
P-O4	1.541(2)
P-O2	1.544(2)
P-O3	1.546(2)
Mean	1.540
T-O-T angles	-100 °C
P O1 Zn	132.03(13)
P O2 Zn	119.84(12)
P O4 Zn	130.86(13)
Mean T-O-T	127.58

Table 5

Table 5a. Hydrogen bond distances (Å) and O-H···O angles (°) at room temperature. H positions were determined with the restraint O-H is 0.95(1) Å and H-H = 1.59(5) Å. D: donor; A: acceptor.

Species	D-H	H…A	D…A	<(DHA)	Hydrogen bond
OH	0.940(10)	1.888(13)	2.811(2)	166(4)	OH1-H1···H_2O1
OH	0.940(10)	1.829(12)	2.7568(18)	169(3)	OH2-H2···O2
OH	0.941(10)	1.888(10)	2.8286(18)	179(3)	OH3-H3···O1
H_2O	0.937(10)	2.451(13)	3.373(2)	168(3)	H_2O1-H4···O2
H_2O	0.940(10)	1.705(13)	2.626(2)	166(3)	H_2O1-H5···OH2
H_2O	0.938(10)	2.07(2)	2.8958(19)	146(3)	H_2O2-H6···O3
H_2O	0.941(10)	1.736(15)	2.646(2)	162(4)	H_2O2-H7···O4

Table 5b. Hydrogen bond distances (Å) at 200 °C, D:donor; A: acceptor.

Species	D-H	D…A	Hydrogen bond
OH	0.95*	2.96	OH1-H1···OH2
OH	0.95*	2.87	OH2-H2···O2
OH	0.95*	2.82	OH3-H3···O1
H_2O	0.95*	2.82	H_2O1-H4···O3
H_2O	0.95*	2.87	H_2O1-H5···O2

* D-H was fixed.

Table 6: For deposit

Table 6. Interatomic distances (Å) and T-O-T angles (°) of veszelyite under ambient conditions and after partial dehydration at 200 °C.

Cu1 coordination	RT	200 °C
Cu1-OH2	1.9308(12)	1.940(8)
Cu1-OH3(2×)	1.9681(12)	1.981(7)
	1.9963(13)	1.986(8)
Cu1-OH1	1.9814(14)	1.962(9)
Cu1-O3	2.4541(12)	2.375(8)
Cu1-H_2O2	2.6164(16)	
Mean	2.158	2.049
Cu2 coordination	RT	200 °C
Cu2-OH2	1.9497(13)	1.954(9)
Cu2-O3	1.9862(13)	1.962(8)
Cu2-OH3	2.0419(12)	2.006(7)
Cu2-OH1	2.0455(12)	2.068(8)
Cu2- H_2O2	2.3385(17)	
Cu2-H_2O1	2.4441(16)	2.248(10)
Mean	2.134	2.048
Zn coordination	RT	200 °C
Zn-O1	1.9304(13)	1.941(8)
Zn-O4	1.9309(12)	1.926(9)
Zn-O2	1.9520(13)	1.905(8)
Zn-OH1	1.9670(13)	1.984(9)
Mean	1.945	1.939
P coordination	RT	200 °C
P-O1	1.5300(14)	1.525(9)
P-O4	1.5380(13)	1.491(9)
P-O2	1.5402(13)	1.524(9)
P-O3	1.5456(13)	1.554(9)
Mean	1.538	1.523
T-O-T angles	RT	200 °C
P O1 Zn	132.42(8)	135.6(5)
P O2 Zn	120.59(8)	123.1(5)
P O4 Zn	131.23(9)	127.5(6)
Mean T-O-T	128.08	128.73

This is a preprint, the final version is subject to change, of the American Mineralogist (MSA)
Cite as Authors (Year) Title. American Mineralogist, in press.
(DOI will not work until issue is live.) DOI: http://dx.doi.org/10.2138/am.2013.4465

Table7: For deposit

Table 7. Results of bond valence calculations for veszelyite RT (a) and 200 °C (b), parameters from Brown and Altermatt (1985).

(a)

Site	O1	O2	O3	O4	OH1	OH2	OH3	H_2O1	H_2O2	Bvs[#]
Cu1			0.12		0.44	0.51	0.44 $2\times\rightarrow\downarrow$		0.08	2.03
Cu2			0.44		0.37	0.48	0.38	0.13	0.17	1.97
Zn	0.54	0.51		0.54	0.49					2.08
P	1.27	1.23	1.21	1.24						4.95
H1					0.81			0.19		1
H2		0.20				0.80				1
H3	0.19						0.81			1
H4		0.09						0.91		1
H5						0.24		0.76		1
H6			0.15						0.85	1
H7				0.23					0.77	1
Bvs[#] without H	1.81	1.74	1.77	1.78	1.30	0.99	1.26	0.13	0.25	
Bvs[#] with H	2.00	2.03	1.92	2.01	2.11	2.03	2.07	1.99	1.87	

(b)

Site	O1	O2	O3	O4	OH1	OH2	OH3	H_2O1	Bvs[#]
Cu1			0.15		0.47	0.49	0.44 $2\times\rightarrow\downarrow$		1.99
Cu2			0.47		0.35	0.48	0.41	0.22	1.93
Zn	0.53	0.58		0.55	0.47				2.13
P	1.28	1.29	1.19	1.41					5.17
H1					0.86	0.14			1
H2		0.16				0.84			1
H3	0.18						0.82		1
H4			0.18					0.82	1
H5		0.16						0.84	1
Bvs[#] without H	1.81	1.87	1.81	1.96	1.29	0.97	1.29	0.22	
Bvs[#] with H	1.99	2.19	1.99	1.96	2.15	1.95	2.11	1.88	

[#] bond valence sum (Brown and Altermatt 1985)

Note: $2\times\rightarrow\downarrow$ indicates that the bv value of 0.44 should be considered twice horizontally and vertically.

Table 8. Observed Raman bands (cm^{-1}) and possible assignments in the spectrum of veszelyite at ambient conditions.

band	assignment	band	assignment
111		833	ν_1(PO)s
115		882	
124		929	
130		951	
143		967	
151		1025	ν_3(PO)a
152		1045	
164		1108	
174	ν(Zn-O), ν(Cu-O), lattice	1379	overtones?
189		1587	ν(OH), ν(H_2O)?
197		1632	
199		1805	
243		1970	
261		2042	
278		2233	
318		2664	ν_s(OH)
364		2852	
377		3184	
387		3286	
439	ν_2(OPO)s	3302	
470		3497	
486		3425	
539	ν_4(OPO)a	3566	
556		3390	
607		3555	
624			

Table 9: For deposit

Table 9. The ratios L/S of the longest to the shortest cross-sections of eight-membered rings of veszelyite at different temperature.

	RT	200 °C
Tetrahedral sheet	2.16	2.27
Octahedral sheet	1.28	1.57

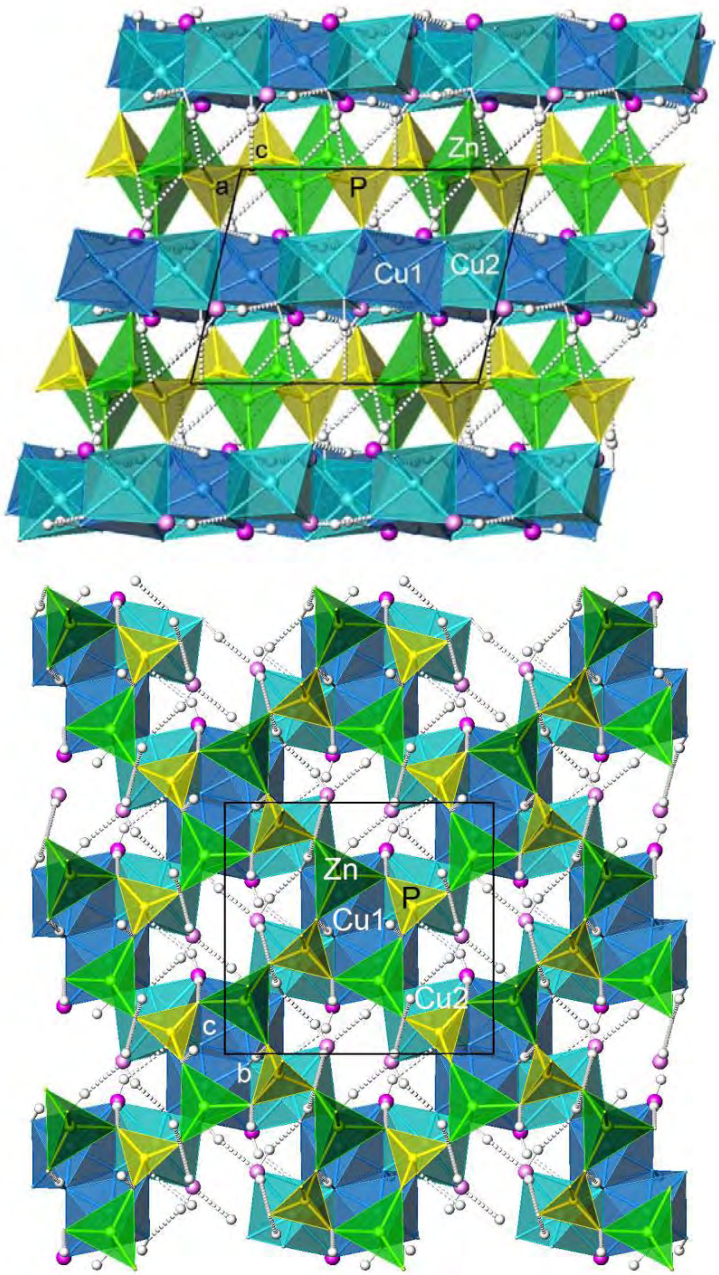

Figure 1. Structure of veszelyite at room temperature. The green tetrahedra represent Zn, while PO_4 tetrahedra are yellow. Octahedra around Cu2 are light blue and octahedra around Cu1 are dark blue. H_2O molecules are shown as pink spheres with attached small white spheres representing H. Hydrogen-bond acceptor interactions are shown by gray dashed connectors. (a) Projection along the **b** axis showing the tetrahedral and octahedral sheets, (b) view of the veszelyite structure parallel to **a** showing the four- and eight-member rings of tetrahedra overlapping the eight-member rings of octahedra.

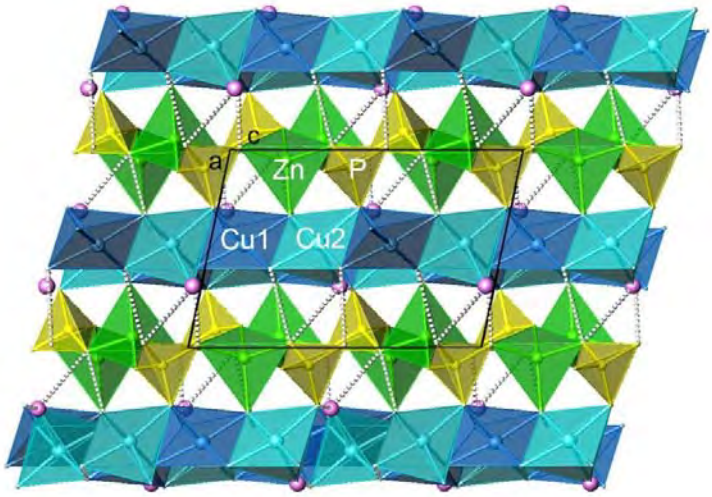

(a)

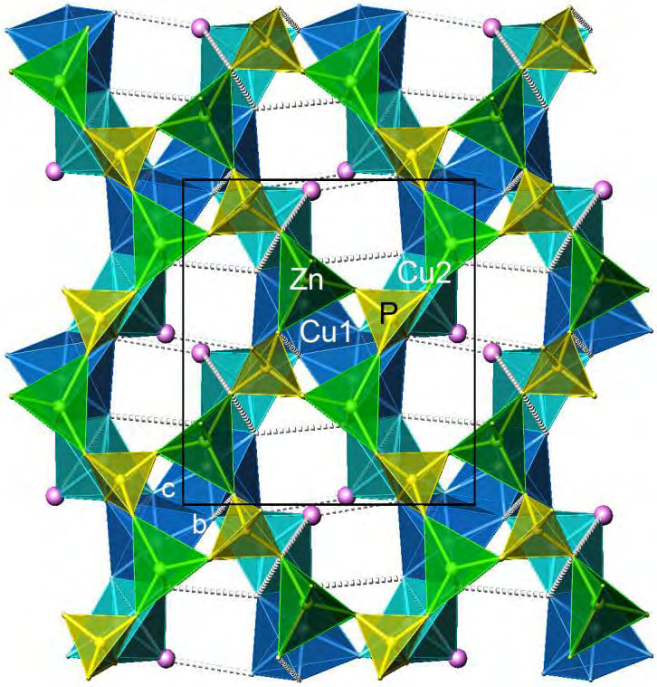

(b)

Figure 2. Structure of veszelyite at 200 °C. (a) Projection along the **b** axis, (b) View of the veszelyite structure parallel to **a**. Colors as in Fig. 1.

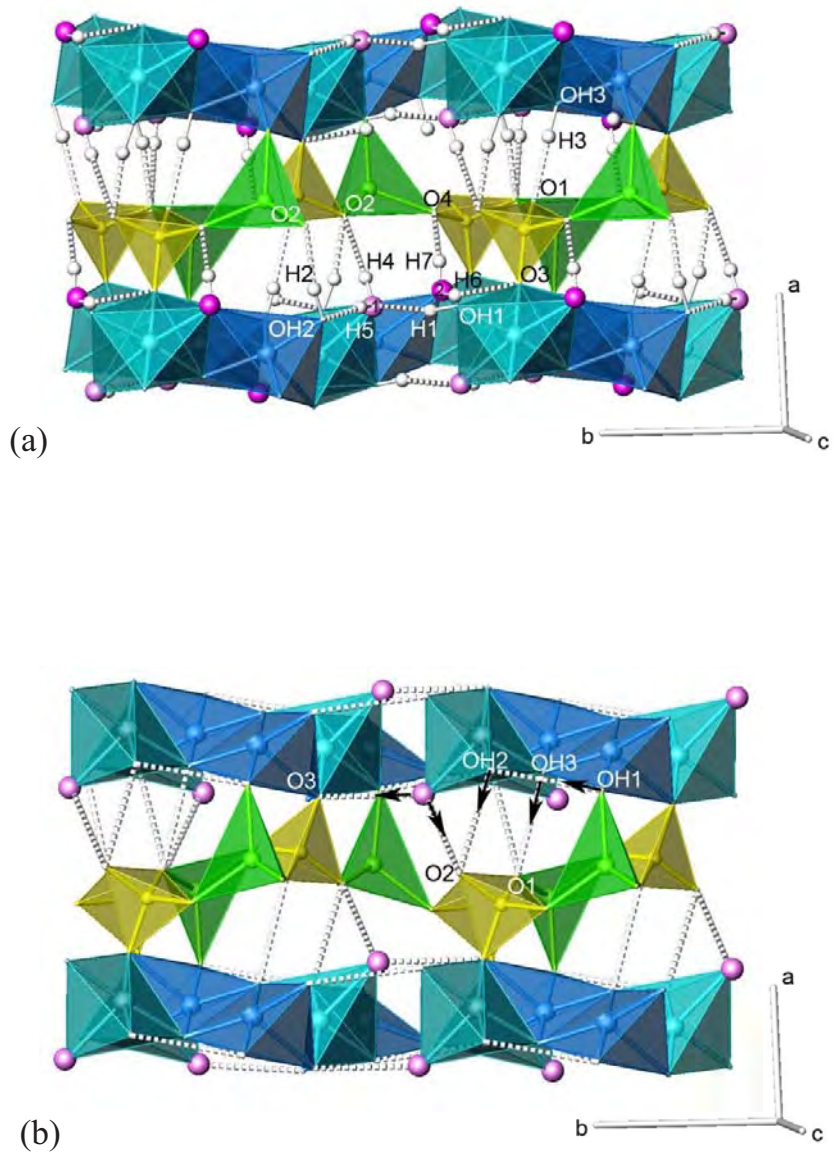

Figure 3. Hydrogen-bond system of veszelyite. (a) Hydrogen bonding at RT. H_2O molecules are shown as pink spheres and the numbers 1 and 2 refer to H_2O1 and H_2O2 sites, respectively. (b) Hydrogen bonding at 200°C, the black arrows indicate the direction to the acceptor. Colors as in Fig. 1.

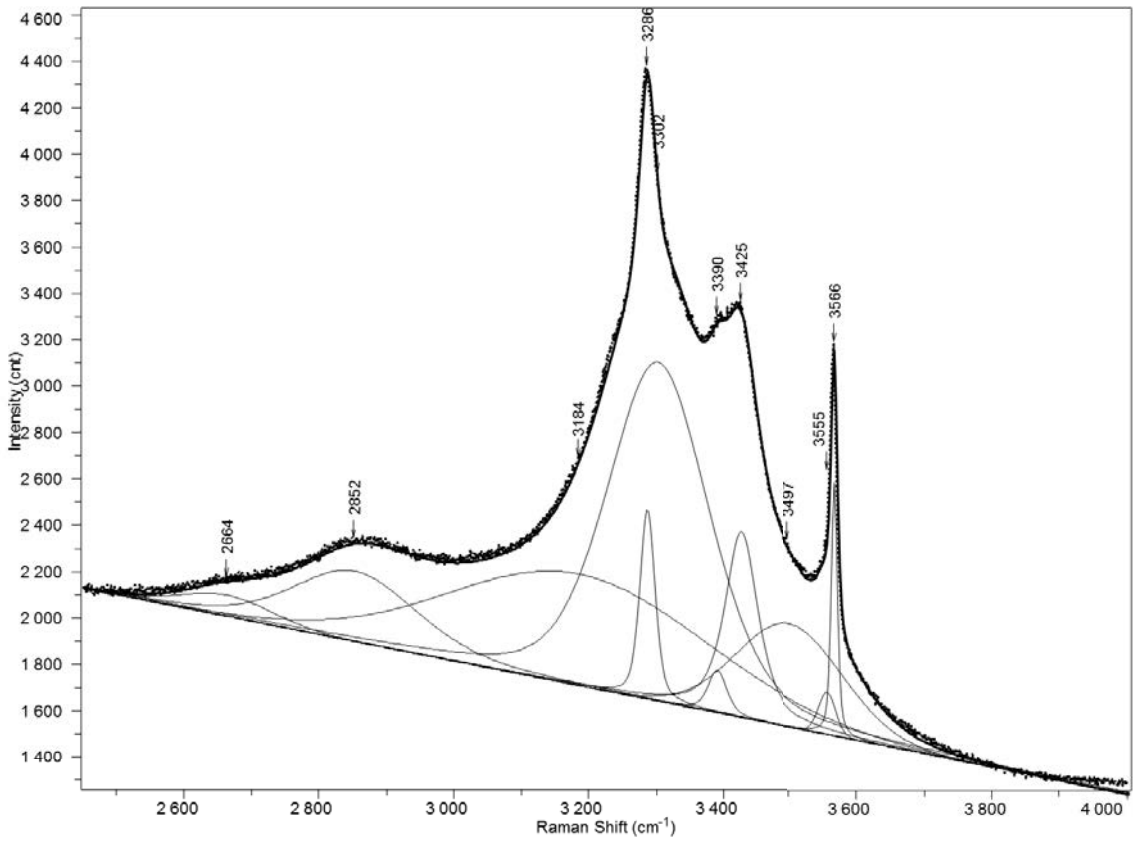

Figure 4. Deconvolution of the Raman spectrum of veszelyite in the range 2500 – 4000 cm^{-1}. Dots – measured Raman spectrum, thin curves – fitted Gauss-Lorentz functions, thick curve – sum curve of fitted functions.

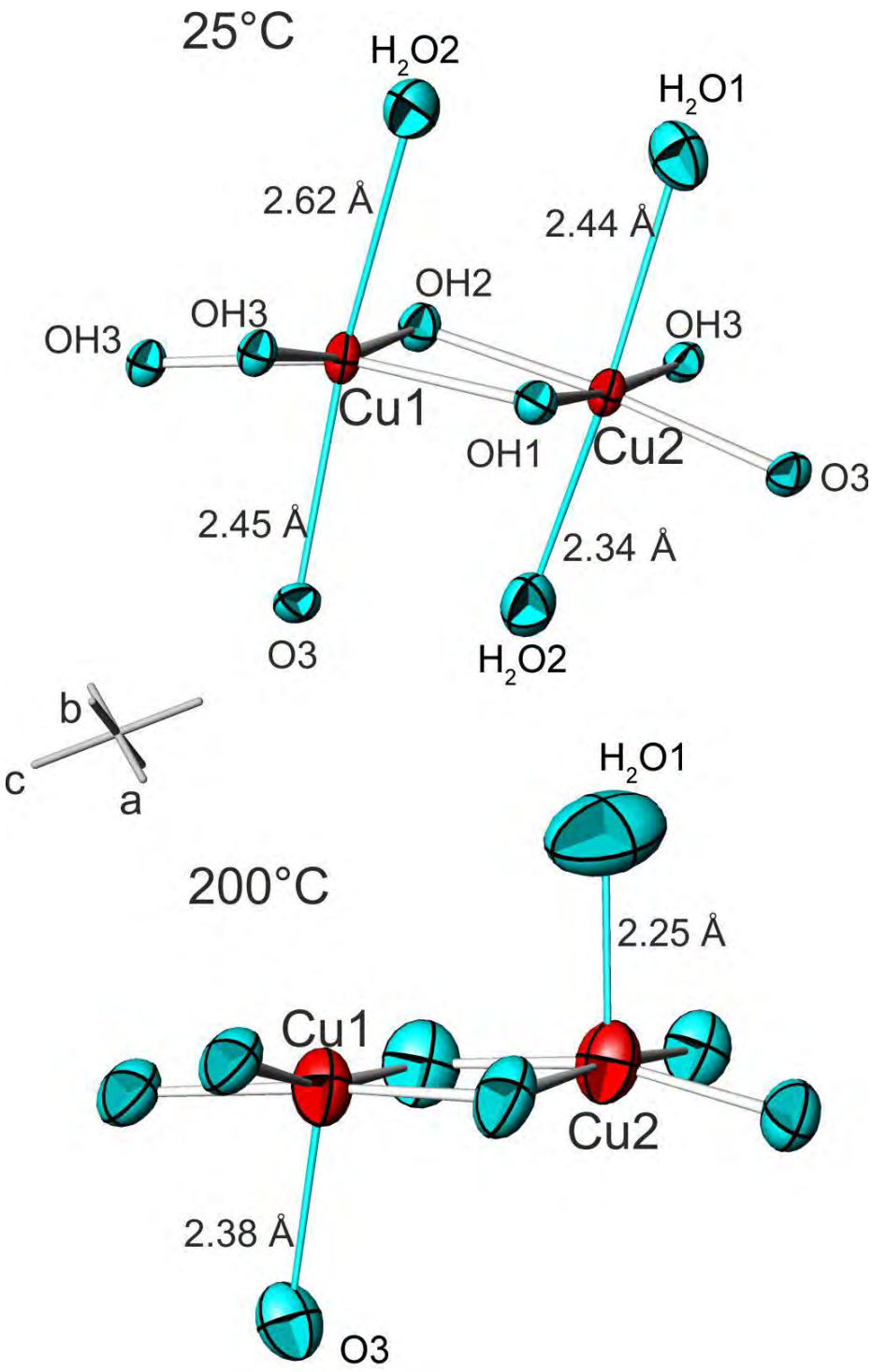

Figure 5: Displacement ellipsoids for Cu1 and Cu2 polyhedra in veszelyite at RT and 200 °C. The probability for ellipsoids is 0.75.

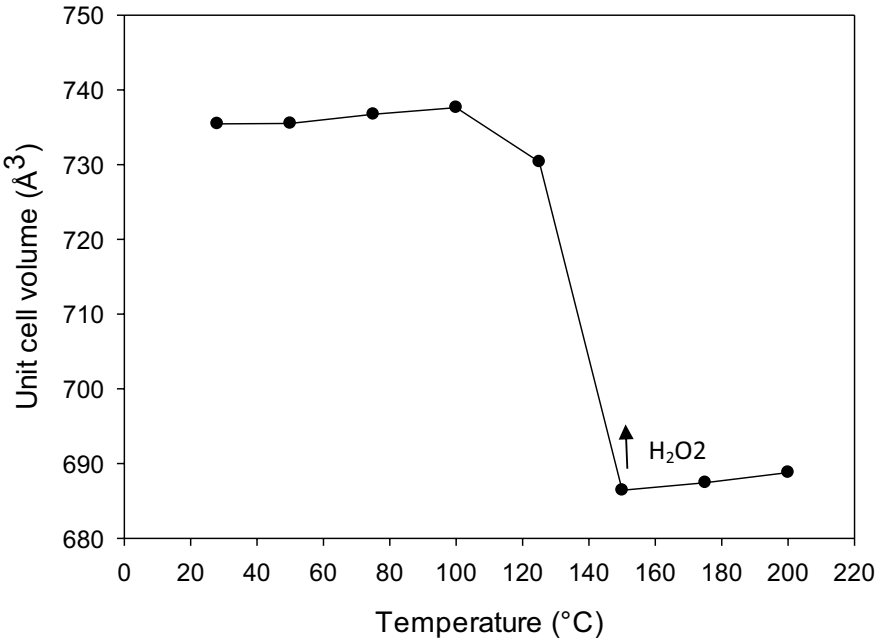

Figure 6. Development of unit-cell volume versus temperature for in situ dehydration experiments of veszelyite. The size of the symbols is larger than the associated esd's.

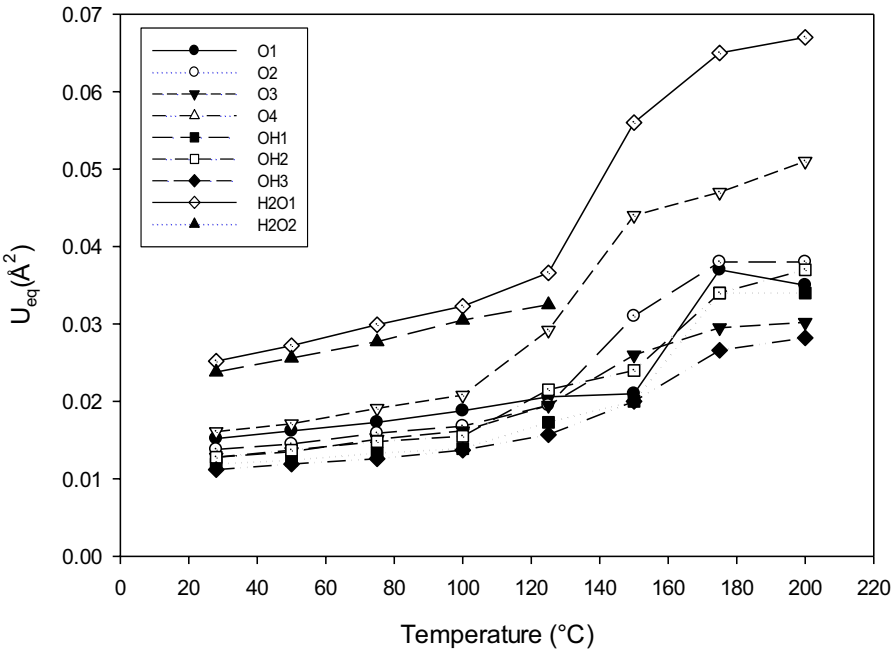

Figure 7. U_{eq} for oxygen sites at different temperatures for veszelyite. The size of the symbols is larger than the associated esd's

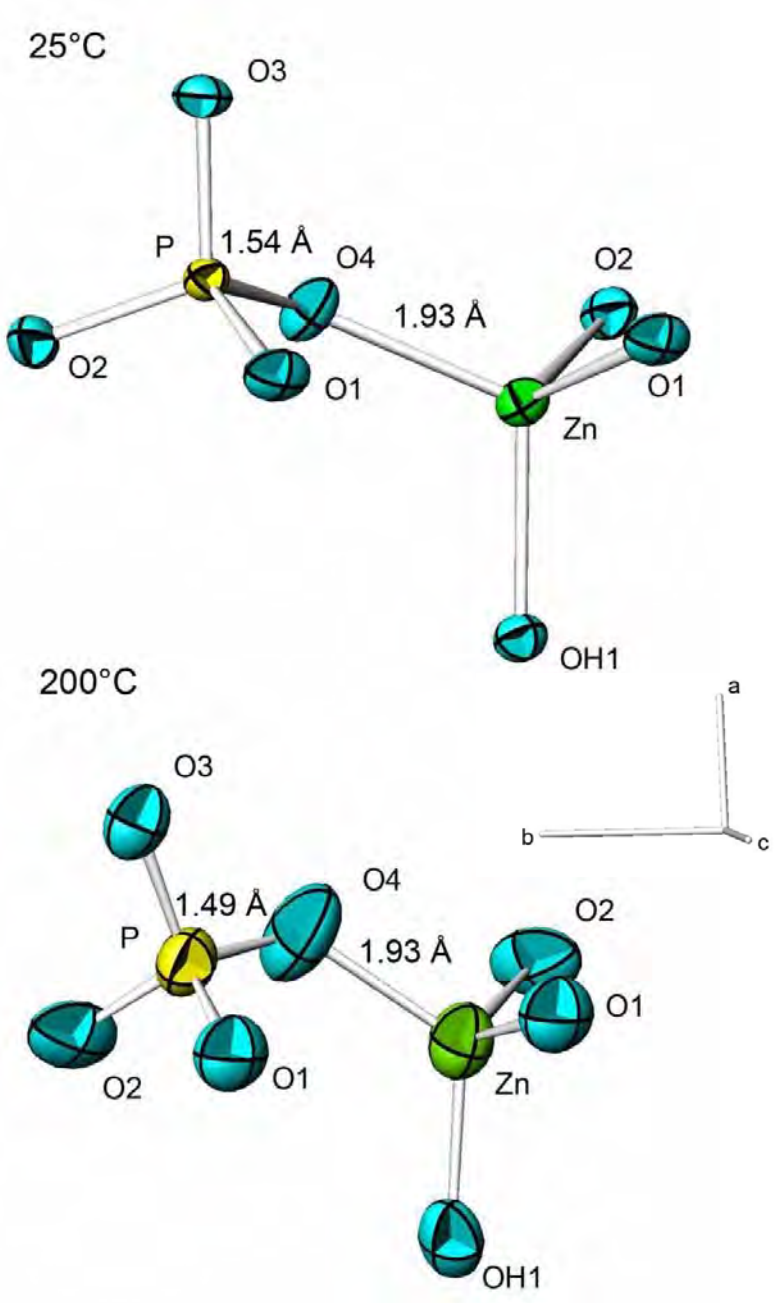

Figure 8: Thermal ellipsoids for P and Zn polyhedra in veszelyite at RT and 200 °C. The probability for ellipsoids is 0.75.

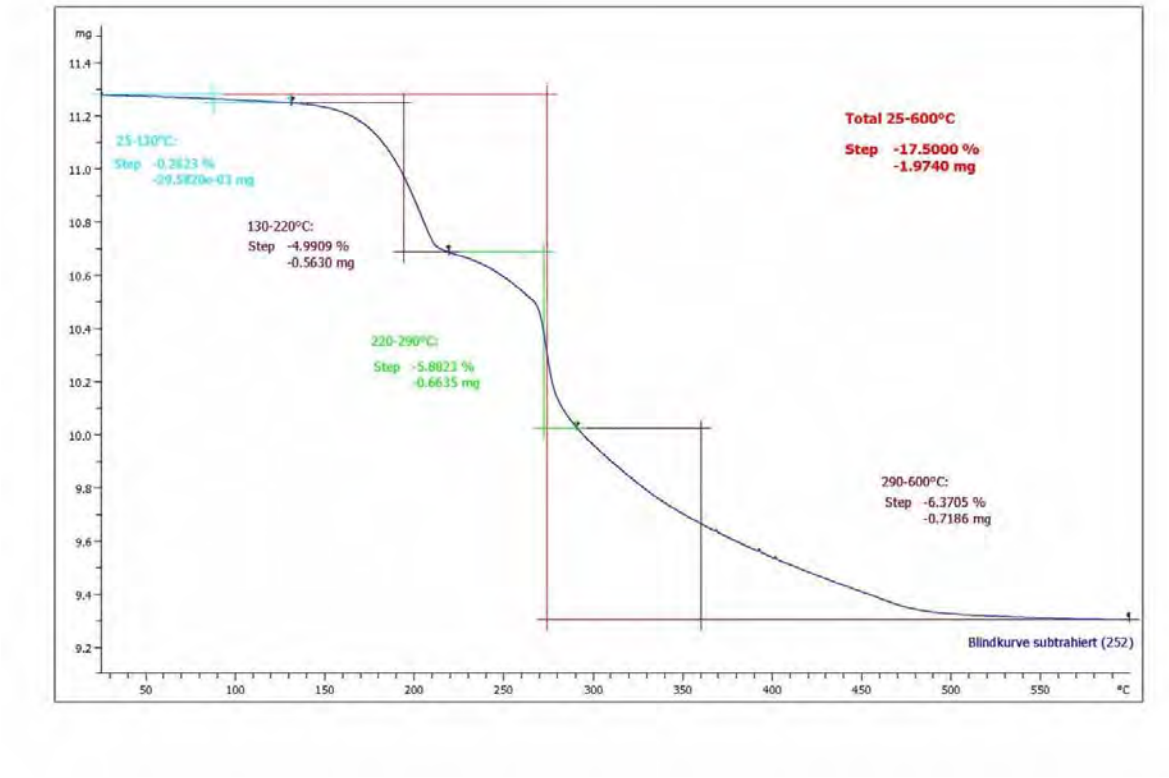

Figure 9 (deposited): Weight curve and calculated mass loss of veszelyite .